CINTAL - Centro de Investigação Tecnológica do Algarve

Universidade do Algarve

SeaGrass Workshop Sea trial

Data report

P. Felisberto, F. Zabel, C. Martins

Rep 04/11 - SiPLAB
October/2011

University of Algarve
Campus de Gambelas
8005-139 Faro,
Portugal

tel: +351-289800131
fax: +351-289864258
cintal@ualg.pt
www.cintal.ualg.pt

Work requested by	CINTAL Universidade do Algarve, FCT - Campus de Gambelas 8005-139 Faro, Portugal Tel/Fax: +351-289864258, cintal@ualg.pt, www.cintal.ualg.pt
Laboratory performing the work	SiPLAB - Signal Processing Laboratory Universidade do Algarve, Campus de Gambelas, 8005-139 Faro, Portugal tel: +351-289800949, info@siplab.fct.ualg.pt, www.siplab.fct.ualg.pt MarSensing Lda Centro Empresarial Gambelas Campus de Gambelas Pavilhão A-5, Sala5.1 8005-139 Faro, Portugal tel: +351-9137229660, contact@marsensing.com www.marsensing.com
Projects	COST (European Cooperation in the Field of Scientific and Technical Research) Action ES0906 (Seagrass productivity: from genes to ecosystem management)
Title	SeaGrass Workshop sea trial:data report
Authors	P. Felisberto, F. Zabel, C. Martins
Date	October, 2011
Reference	04/11 - SiPLAB
Number of pages	42 (forty two)
Abstract	The Seagrass Workshop sea trial took place in a very shallow water area in front of STARESO (Station the recherches sous-marines et oceanographiques), Punta la Revellata, Gulf of Calvi, Corsica from 10 to 19 October 2011, in the framework of the Action ES0906 (Seagrass productivity: from genes to ecosystem management) supported by the FP7 Programme COST (European Cooperation in the Field of Scientific and Technical Research). During this multidisciplinary workshop the participating groups have sampled the Posidonia oceanica field using different methods in order to characterize the seagras individuals and the whole community. This report describes the data gathered by the SiPLAB/Marsensing team, which objective is to characterize the influence of seagrass oxygen production in acoustic propagation and develop techniques to estimate oxygen production by acoustic means.
Clearance level	UNCLASSIFIED
Distribution list	SiPLAB(1+2DVDs), Marsensing (1+2DVS), CINTAL (1+2DVDs), Seagrass Group(1+2DVDs)
Total number of copies	4 (four)

Contents

List of Figures

Abstract

The Seagrass Workshop sea trial took place in a very shallow water area in front of STARESO (Station the recherches sous-marines et oceanographiques), Bay of la Revellata, Calvi, Corsica from 10 to 19 October 2011, in the framework of the Action ES0906 (Seagrass productivity: from genes to ecosystem management) supported by the FP7 Programme COST (European Cooperation in the Field of Scientific and Technical Research). The Posidonia oceanica is a seagrass that covers large littoral areas of the Mediterranean. Posidonia meadows are an habitat for different marine species and its productivity is related to the health of the environment. During this multidisciplinary workshop the participating groups have sampled the Posidonia oceanica field using different methods in order to characterize the seagras individuals and community as a whole. This report describes the data gathered by the SiPLAB/Marsensing team, which objective is to characterize the influence of seagrass oxygen production in acoustic propagation and develop techniques to estimate oxygen production by acoustic means.

This report presents the experimental setup, the acoustic and complementary environmental data acquired during the sea trial, and discusses preliminary results of channel characterization. This work was partially supported by the FP7 Programme COST project Action ES0906 and FCT (ISR/IST plurianual funding) through the PIDDAC Program funds.

Acknowledgments

The authors thank Prof. Rui Santos for the invitation to participate in this workshop, technical and scientific staff at STARESO, specially Sylvie Gobert, for the logistics, at sea operations, meteorological and CTD data, and Marsensing for the self-recording hydrophones. This work was partially supported by the FP7 Programme COST project Action ES0906 and FCT (ISR/IST plurianual funding) through the PIDDAC Program funds.

Chapter 1

Introduction

It is expected that the oxygen production by Posidonia oceanica meadows give rise to changes in the acoustic signature of signals that propagate through the meadow[1, 2]. An increase of oxygen production by the algae should lead to higher attenuation of the received signal. In the underwater multipath environment, the arrival structure (number of echoes and their strength) will be modulated by the concentration of oxygen in the water. Since the oxygen production is linked to photosynthesis, the arrival structure observed during the night (no light, no photosynthesis, no oxygen production) will differ from that observed during the day (high photosynthesis activity, high oxygen production). However, when the sound propagates through the ocean it is also influenced by other environmental parameters (one assumes that the geometry is fixed) like wind speed, temperature, among others, that also gives rise to changes in the arrival structure in time scales comparable with that of oxygen production. The potential acoustic methods developed to quantify the oxygen production should in a first step track the changes in the arrival structure and be able to separate (filter out) the changes due to oxygen production from those due to other environmental variations. Once the tracking procedure is achieved the next step is to relate the changes observed in the arrival structure to the produced amount of oxygen. This quantification procedure should be calibrated with other independent methods, what is in general a not so simple task, since acoustics gives integral information, whereas alternative methods gives local information.

In the literature one can find two type of acoustic based methods for characterization of acoustic production of a seagrass meadow:

1. Survey the seagrass prairie using a sidescan sonar. Allows for point characterization.
2. Acoustic transmission between a moored sound source transmitting a predefined signal to a vertical array moored at hundreds of meter position. Allows for integral characterization (oxygen consumption/release changes) of the meadow along the acoustic path during the dial (24 hours) cycle.

The experiment reported herein is focussed on the latter method. The method was previously investigated by Hermand [1, 2], who showed its potential to characterize the oxygen consumption/release changes of a seagrass meadow continuously during several days. The method showed the correlation between changes in the received acoustic signal (channel impulse response) and oxygen production of the seagrass meadow. The goal is to quantify the oxygen changes from the acoustic channel changes, giving rise to a low cost method for long term observation of the seagrass meadow.

This report is organized as follows: in the next chapter the experimental setup is presented. In chapter 3 the environmental data gathered is discussed, whereas in chapter 4

the acoustic data is shown. Chapter 5 presents preliminary results of acoustic channel characterization, its relation to oxygen production and discusses ways for further processing. Conclusions are drawn in chapter 6.

Chapter 2

The experimental setup

The Seagrass Workshop sea trial took place in a very shallow water area (< 25 m water depth) in front of STARESO (Station the recherches sous-marines et oceanographiques), Bay of Revellata, Calvi, Corsica from 10 to 19 October 2011. The acoustic data were acquired in two periods: first period began at 11 October evening and finished at 14 October evening, whereas the second began 16 October morning and finished at 18 October evening. Due to bad weather conditions the hydrophones' were recovered from sea between the first and the second period. The acoustic monitoring system was composed by a sound source to transmit probe signals, installed close to the STARESO pier and 3 self-recording hydrophones moored in Posidonia oceanica meadow at 20 m water depth. The working area and the placement of the acoustic equipment is shown in figure 2.1.

Figure 2.1: Seagrass workshop area showing the source and hydrophones mooring location

The scheme of the acoustic experiment setup is shown in figure 2.2. The source was installed 2 m above the sea bottom in a site with water depth 8.5 m, close to the pier in order to be powered from a 220V power outlet. The hydrophones were moored in 21.5 m water column, 8 m,4 m and 2 m above the sea bottom. The water depth values were obtained by a depth finder (echo sounder) installed in the boat. The distance between the sound source and the hydrophone's mooring was approximately 122 m. Figure 2.3 shows the sound source mooring (a) in the Posidonia oceanica meadow and the hydrophones' mooring (b).

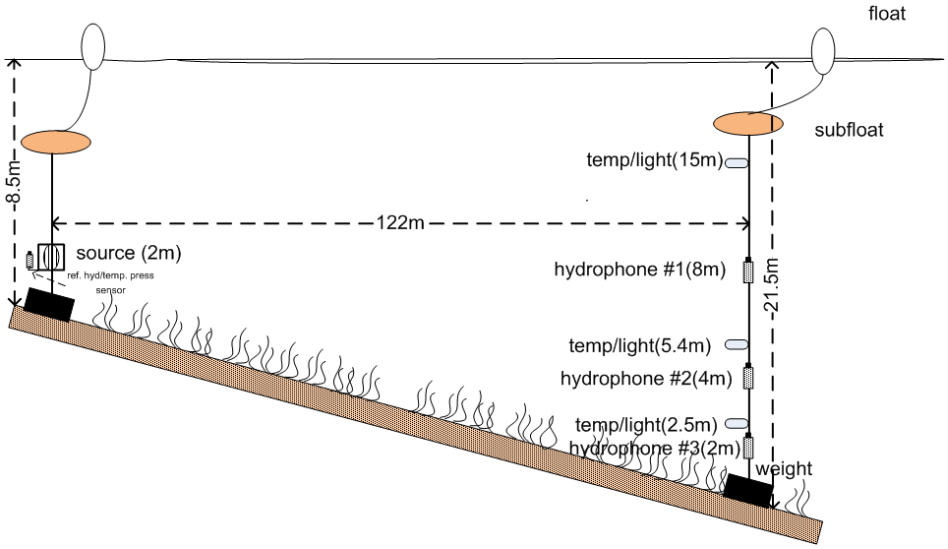

Figure 2.2: Experimental setup. Depths of the sensors measured from the sea bottom.

(a) (b)

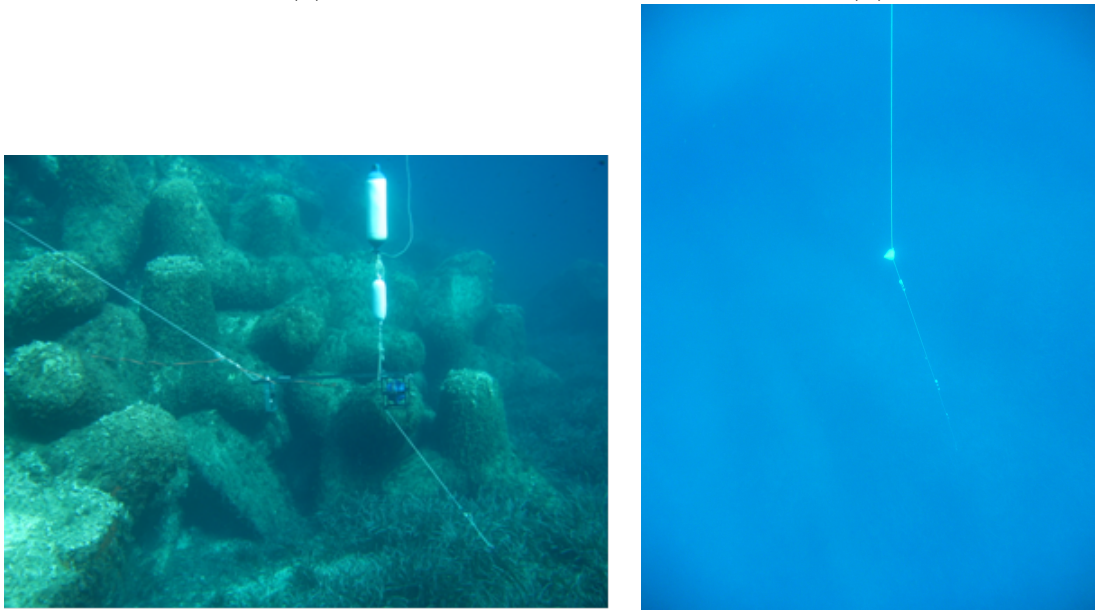

Figure 2.3: Acoustic equipment moorings: (a) sound source mooring showing the subfloat buoy, the sound source and the support for the reference hydrophone (not attached) and temperature/pressure data logger; (b) hydrophones' mooring showing the subfloat buoy and the hydrophones attached to the rope

The sea bottom was densely covered by Posidonia with some gaps at 15 m water depth area. The bottom is sandy with rocky patches. A temperature/pressure sensor was installed in the source mooring and three temperature/light sensors were installed in the hydrophone's mooring at 15 m, 5.4 m and 2.5 m above the sea bottom. During the experiment several CTD measurements were performed close to the hydrophone's mooring, in the middle of the propagation path and close to the source mooring. The next chapters describe the equipments used and the data acquired during the experiment by the oxygen acoustic team: environmental data in chapter 3 and acoustic data in chapter 4.

Chapter 3

Environmental data

This chapter presents atmospheric and underwater environmental data. The atmospheric data was recorded by a meteorological station installed on top of the STARESO building. The underwater data were acquired by a CTD Sea-Bird SBE19, operated from a boat (see fig. 3.1(a)), 3 HOBO Pendant temperature/light data loggers (UA-002) (see fig. 3.1(b)) installed in the hydrophones' mooring at different depths and a HOBO temperature/pressure sensor installed in the source mooring.

(a) (b)

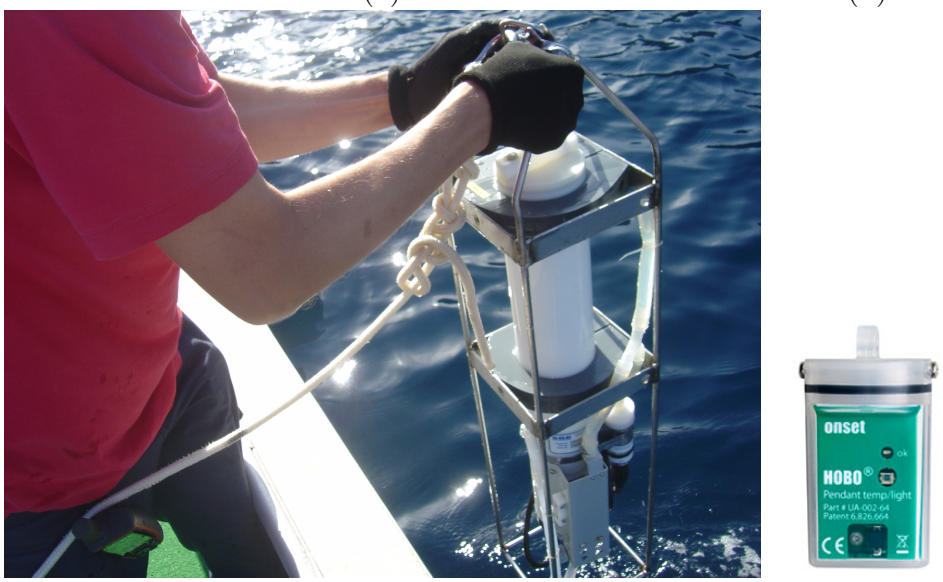

Figure 3.1: The SeaBird CTD operated from the boat (a) and the HOBO temperature/light sensor (b)

3.1 Atmospheric data

Figure 3.2(a) shows the wind speed (plain black line), wind gusts (dotted line) and wind direction (red dots) observed during the period of the experiment. One can notice the bad weather event between October 14 and 16, with wind gusts from NE reaching more than 20m/s in October 15. During this bad weather event the average air temperature fell 5°C, what can be seen in fig. 3.3(a) in addition with the air pressure at sea level.

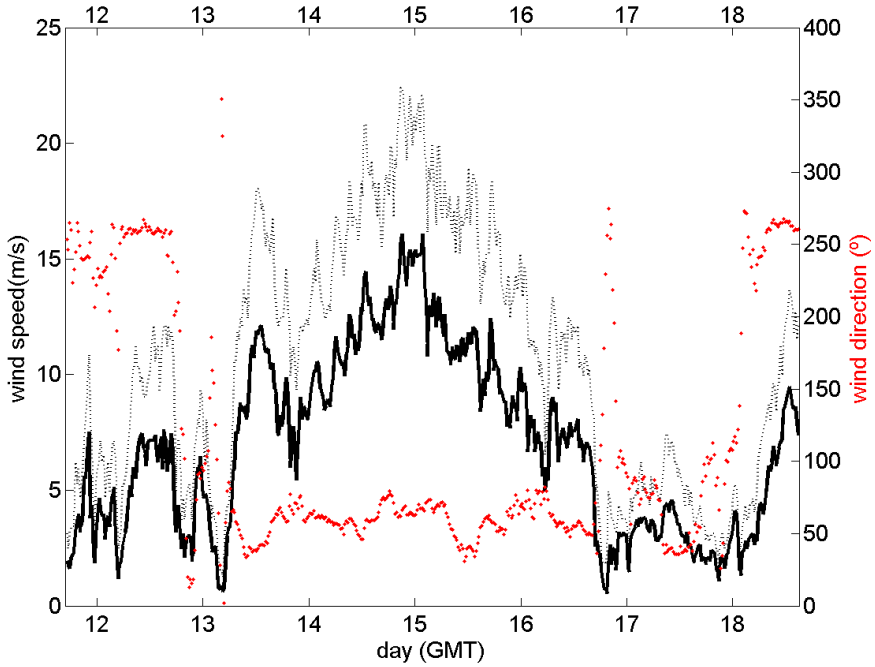

Figure 3.2: Atmospheric data: wind speed (black line), wind gusts(dotted line), wind direction (red dots)

Fig. 3.3(b) shows the humidity and the solar irradiance during the period of the experiment. On can expect that the oxygen production, due to photosynthesis will be highly correlated with irradiance. On can see that in the considered period, the solar irradiance along the day does not show remarkable daily changes.

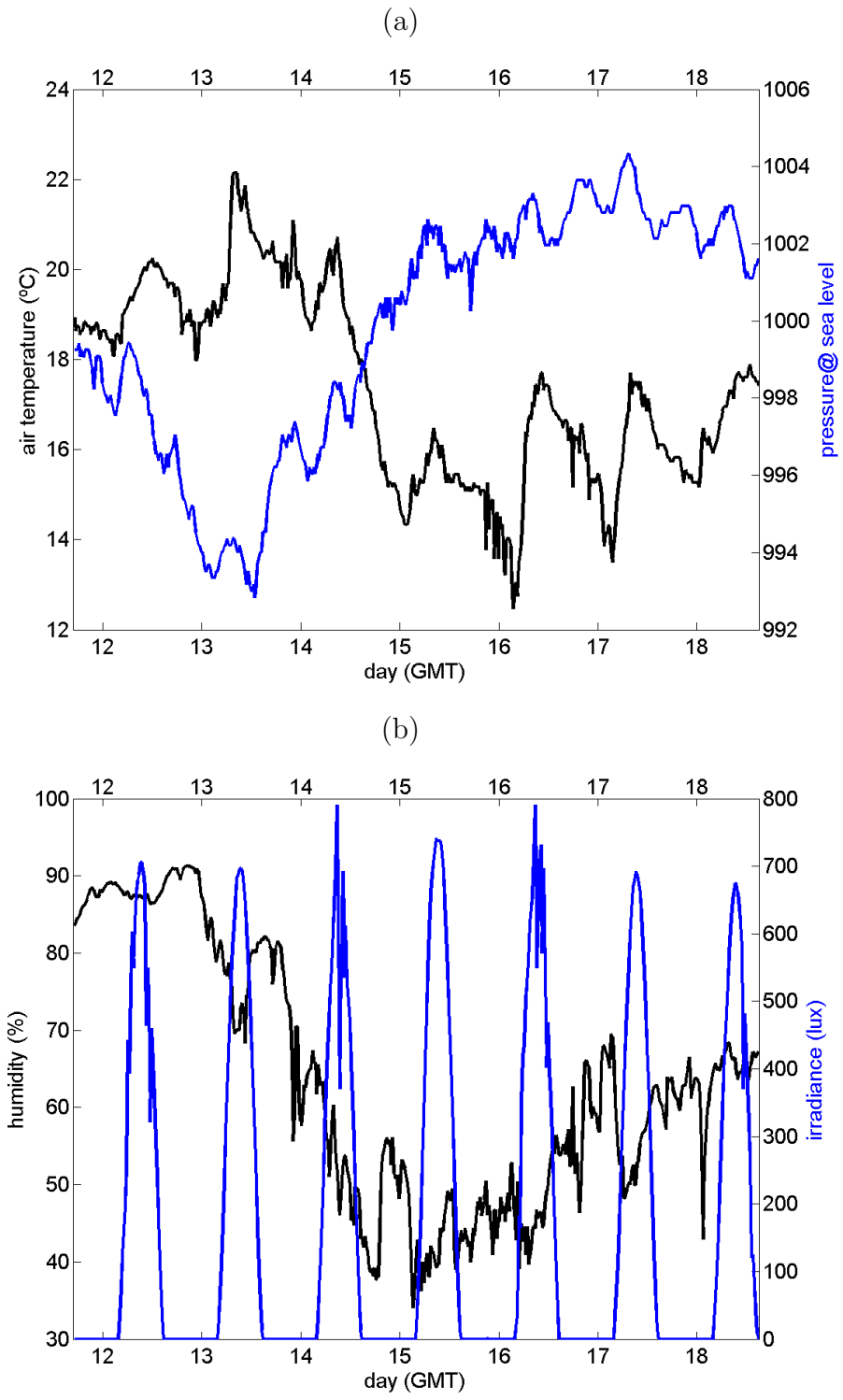

Figure 3.3: Atmospheric data: (a) air temperature (black line), air pressure sea level (blue line); (b) air temperature (black line), solar irradiance (blue line)

3.2 CTD data

Figure 3.4 shows the temperature and salinity data measured by the CTD. Profiles acquired at different days are represented by different colors. The label in format dd-hh at the lower end of the temperature profiles represents the day (dd) and the hour (hh), when

the respective measurement was performed. The profiles with the same color and label where performed at different locations few minutes apart: profiles that reach the deepest value were acquired close to the hydrophone's mooring, whereas those profiles related to shallower value were acquired in a middle position between the source and hydrophones' moorings. During the first and second day some profiles were acquired close to the source mooring (the shallowest profile in a group that shares the same color and label).

(a)

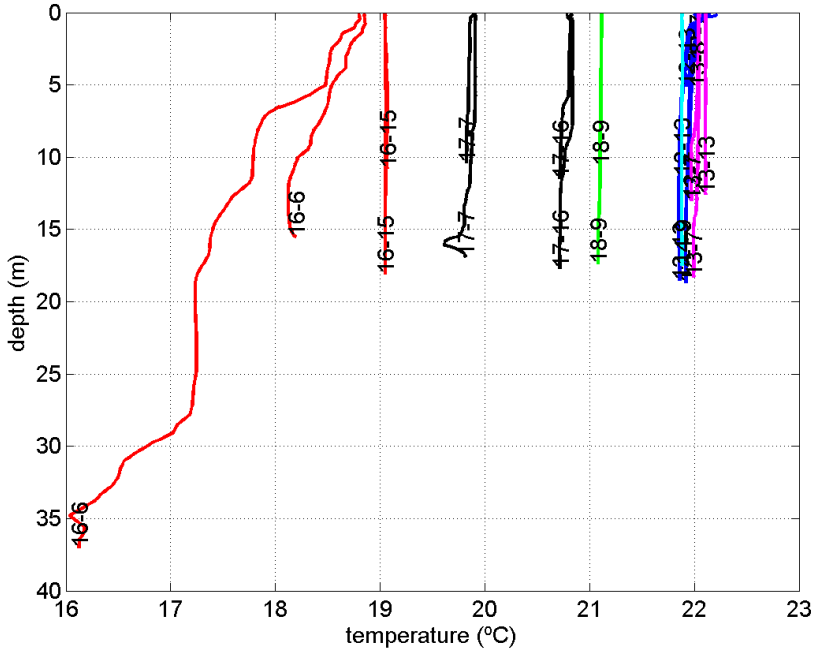

(b)

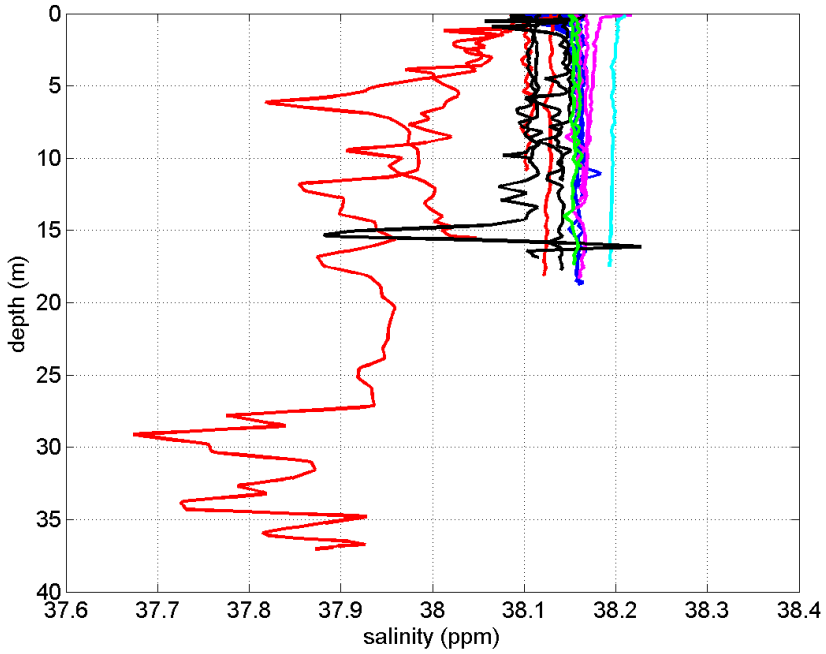

Figure 3.4: Temperature (a) and salinity (b) data from CTD. The text label indicates the day-hour (GMT) of a profile.

Figure 3.5 presents the sound speed profiles computed from temperature/salinity profiles shown in 3.4 using the Mackenzie formula. From the begin of the experiment, October

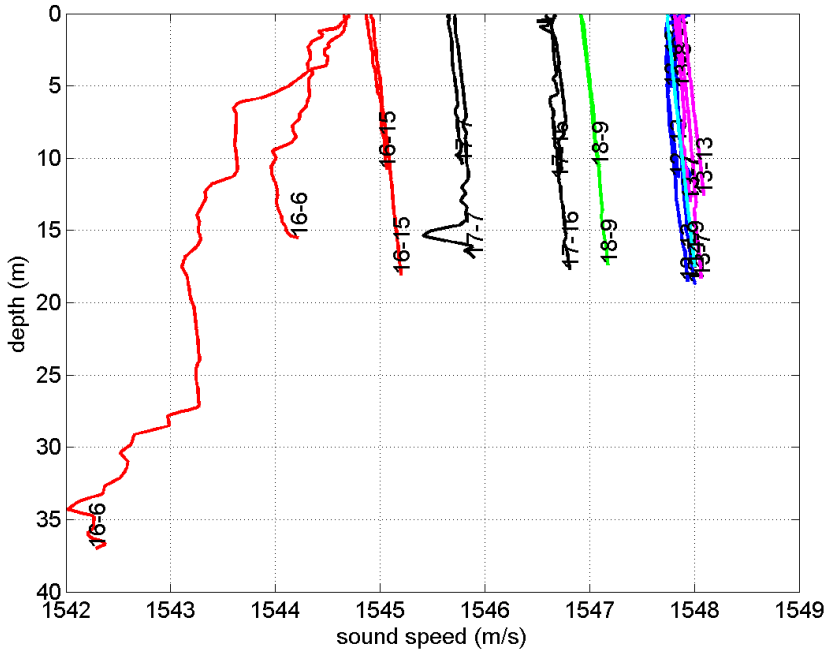

Figure 3.5: Sound speed profiles computed from CTD data (fig 3.4) using the Mackenzie formula

11, to October 13 evening there were good weather conditions. In this period one can notice a an isothermal profile ($\approx 22\,^{o}$C) and constant vertical salinity (≈ 38.1 ppm), giving rise to isovelocity profiles (≈ 1548 m/s). On can also remark that morning and afternoon temperatures changes are not significative. From October 13 evening, the wind speed significantly increased and peak values of 30km/h were reached. For safety reasons during the bad weather period that lasted until 15 October evening, the hydrophones were not deployed and CTD casts were not performed. October 16 morning the weather conditions improved and a CTD cast was performed at 6 am (GMT, 8 am local time), showing the temperature decreasing from 22 ^{o}C before the bad weather event to 18.5 ^{o}C. Moreover the temperature profile is now slightly downward decreasing and the sound speed profile downward refracting. The wind speed and wave height decreased along the day (October 16) and the afternoon profile shows already an isothermal/isovelocity profile and an increasing temperature (sound speed). This trend was observed during the next two days of the experiment.

3.3 Temperature and light intensity

Figure 3.6 presents the temperature (a) and light intensity (b) measured by HOBO data loggers attached to the hydrophones mooring rope at 15 m (blue dots), 5.4 m (red dots) and 2.5 m (black dots) above the sea bottom. Those easy to use sensors have low accuracy (temperature measurement error $\pm 0.5\,^{o}$C) but high sampling rate (one sample per minute), allowing to track significative perturbations in short time scales that may occur, which cannot be sampled by scarce CTD measurements. Herein the temperature sensor data shows that there is no significative day/night changes in the sea water temperature, moreover that the temperature was constant in the period before the bad weather event,

(a)

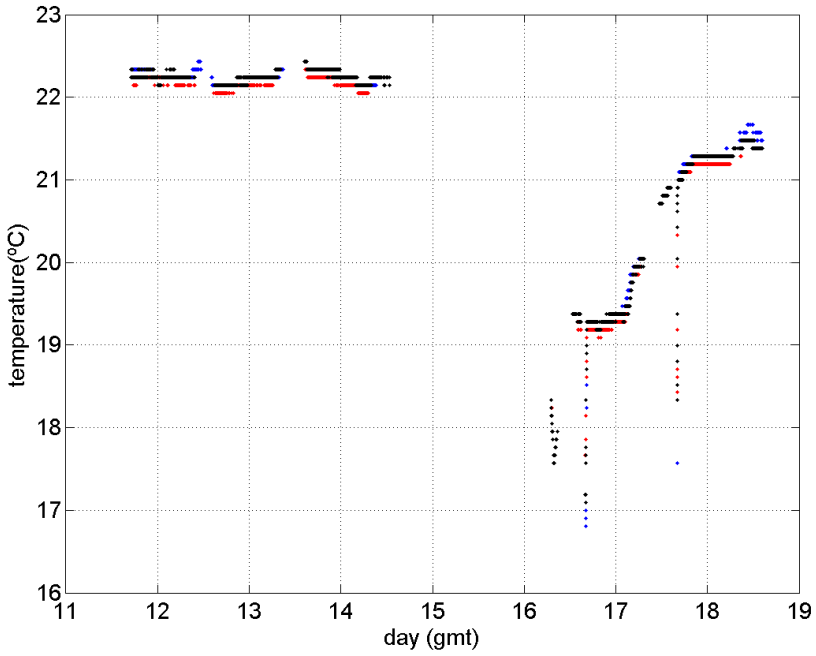

(b)

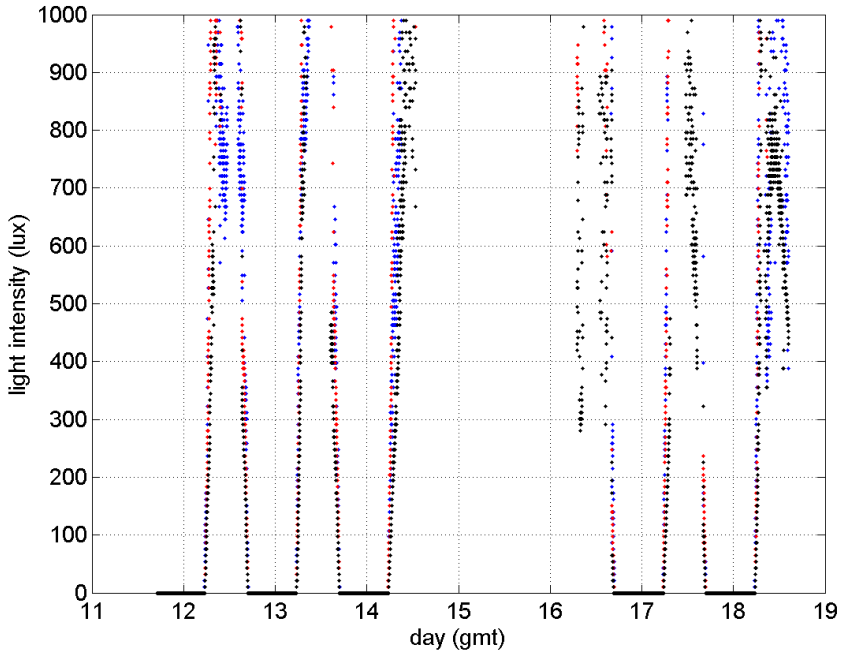

Figure 3.6: Temperature (a) and light intensity (b) acquired at 15 m (blue dots), 5.4 m (red dots) and 2.5 m above the sea bottom

and constantly increased in the period after. The light intensity data clearly shows the sunrise/sunset events, and the steepest increase/decrease of the light intensity after/before those events. One should remark that during the day when the light intensity is above 400-500 lux the measurements show high variability, data dropouts occur, and apparently the values are clipped at 1000 lux. Thus the variation of light intensity with depth is

meaningful only during a short period after sunrise and before sunset. Moreover, the light spectrum measured by those sensors is not well suited to track the photosynthesis process.

3.4 Source depth and temperature

Figure 3.7 presents the data acquired by a HOBO data logger installed in a support attached in front of the source: (a) the depth estimated from pressure data and (b) the temperature. This data logger (and the source) was moored during the whole experiment, including the bad weather period.

In the depth graph one clearly identify the tidal influence, giving rise to a "sinusoidal" low-frequency variation with a period in line with the tidal period. Also, one can identify the bad weather period when high instantaneous perturbations occur, specially from October 14 evening until October 16. Part of the high amplitude of these perturbations is also related with the mooring, since for safety reasons the tension on the ropes where diminished at the beginning of the bad weather event and a suddenly shift of the depth occurred. When the weather improved the initial conditions of the mooring were restored, but a shift of 20 cm towards the surface of the mean source depth (6.7 m) is noticed in this period in comparison with the initial period (6.9 m).

These temperature measurements in addition to the observations based on CTD a temperature sensors in hydrophones mooring show the temperature fall during the bad weather event (not available from the other sensors) and that the minimum of the temperature was reached October 16 at 7h20 GMT (9h20 local time).

(a)

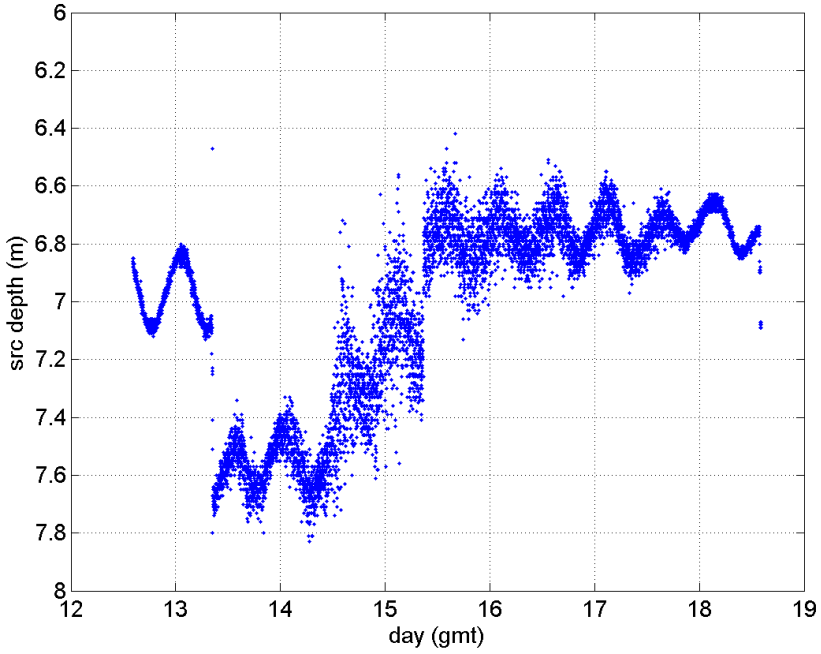

(b)

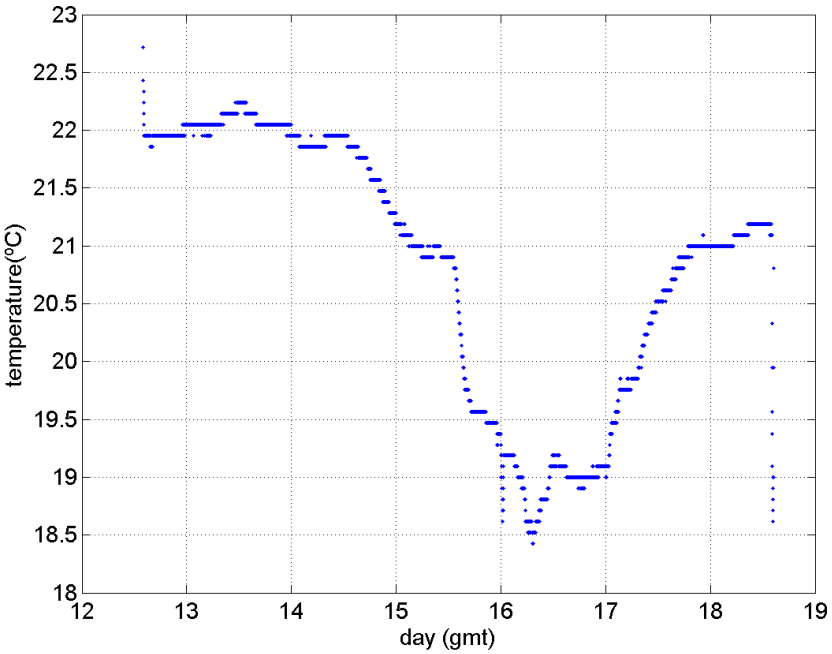

Figure 3.7: Source depth (a) and temperature (b) measured by the HOBO device installed at the source

Chapter 4

Acoustic data

During the experiment, probe signals were transmitted from a sound source at 6.5 m depth to 122 m distant 3 self-recording hydrophones at 2, 4 and 8 m above the sea bottom (see fig. 2.2). The acoustic data were transmitted during two periods of about 2.5 days, separated by the bad weather event. During the first period the transmitted signal sequence was repeated every 15 minutes with two stops for data download, and battery replacement at the lab. In the second period, after the bad weather event, the repetition rate of the transmitted signal sequence was set to 5 minutes, and the endurance of the second hydrophone was increased doubling the number of battery cells. Table 4.1 summarizes the schedule of the acoustic acquisitions.

RUN ID	HYD #	ST (GMT)	ET(GMT)	Rep. RATE (mins)
R11102011	1	11 Oct 17:00	12 Oct 11:30	15
	2	11 Oct 17:00	12 Oct 11:30	15
	3	11 Oct 17:00	12 Oct 00:30	15
R12102011	1	12 Oct 14:00	13 Oct 05:00	15
	2	12 Oct 14:00	13 Oct 9:15	15
	3	12 Oct 14:00	13 Oct 00:15	15
R13102011	1	13 Oct 14:30	14 Oct 04:30	30
		14 Oct 05:00	14 Oct 13:30	15
R16102011	1	16 Oct 07:00	16 Oct 15:00	5
	2	16 Oct 07:00	16 Oct 15:00	5
	3	16 Oct 07:00	16 Oct 15:00	5
	SRC	16 Oct 10:30	16 Oct 15:50	5
R16102011_NOITE	1	16 Oct 16:00	17 Oct 15:54	5
		17 Oct 03:00	17 Oct 13:20	5
	2	16 Oct 16:00	17 Oct 14:30	5
	3	16 Oct 17:00	17 Oct 01:15	5
R17102011	1	18 Oct 03:00	18 Oct 14:40	5
	2	17 Oct 16:00	18 Oct 14:40	5
	3	17 Oct 16:00	18 Oct 00:15	5

Table 4.1: Table of acoustic acquisitions with columns: RUN ID, run identification; HYD, hydrophone number in the array (1,2,3) or at the source (SRC); ST and ET, daytime (GMT) at the start, respectively at the end of the run ; Rep. RATE, repetition rate of transmissions

4.1 The acoustic emission/reception system

The system used to transmit the probe signals was composed by the Portable Acoustic Source Unit System (PASU)[3] acting as a signal generator and signal amplifier, and the sound source Lubell LL916C Underwater Speaker. The amplifier gain was set to attain the maximum source power available for the signal sequence considered. A reference hydrophone digitalHyd SR-1 supplied by Marsensing Lda was attached to the source mooring, however it acquired data only during a 5 hour period (see table 4.1 for details). The receiving system was composed by 3 self-recording digital hydrophones digitalHyd SR-1. Figure 4.1 shows the PASU unit, the Lubell sound source and the 3 digitalHyd SR-1 self-recording hydrophones during equipment preparation before deployment. A detailed description of the source and hydrophones can be find in appendix A and B respectively. In order to minimize the power consumption of the hydrophones, the acquisition was

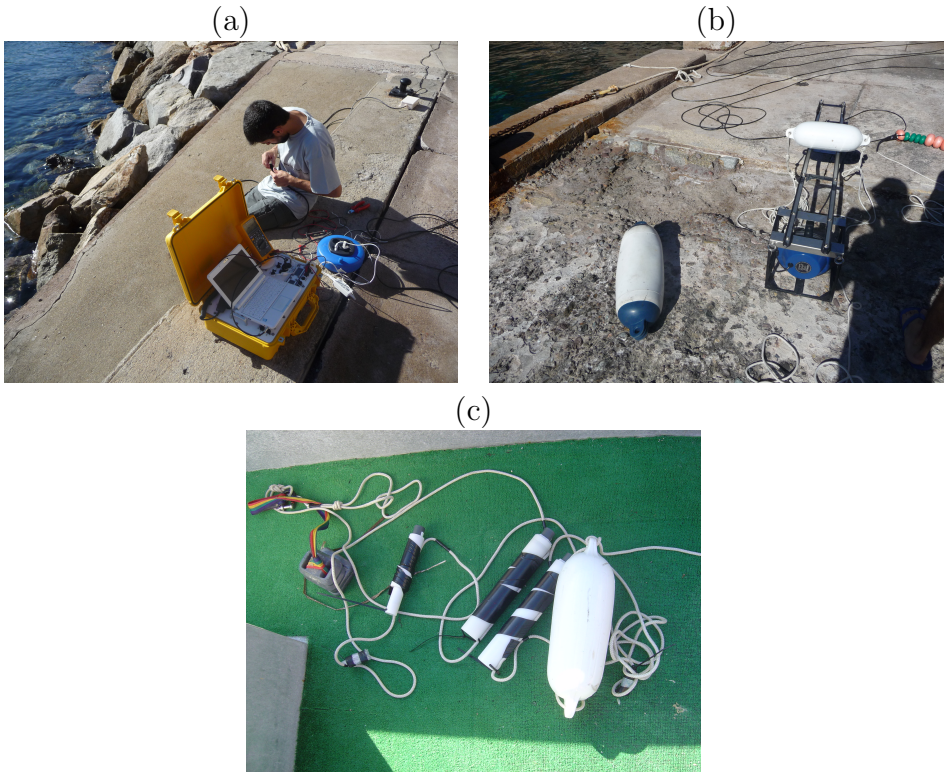

Figure 4.1: Acoustic equipment preparation: (a) PASU unit, (b) Lubell LL916C sound source, (c) Marsensing self-recording digital hydrophones SR-1

performed according a preprogrammed schedule, being the hydrophones in power down between acquisitions. Since the emitted signal sequence was 124.5 s long, the acquisition time was set to 140 s to avoid loss of data due to possible clock offsets between the PASU and the self-recording hydrophones.

4.2 Emitted signals

The sequence of probe signals, transmitted at rate of 44100 samples per second, were composed by 3 groups of several 3 s long chirps, corresponding to three distinct frequency bands: low frequency band 400-800 Hz, medium frequency band 1500-3500 Hz and high frequency band 6500-8500 Hz. The group of low frequency and the group of high frequency

was composed by 12 chirps, the group of middle frequency signals was composed by 10 chirps. The amplitude of the 2 initial chirps was 20 times smaller than the amplitude of the following ones. The groups were separated by 2 s idle, within a group the chirps were 250 ms apart. During the 2nd period of transmissions (after the bad weather event) a communication signal was added at the end of the sequence.

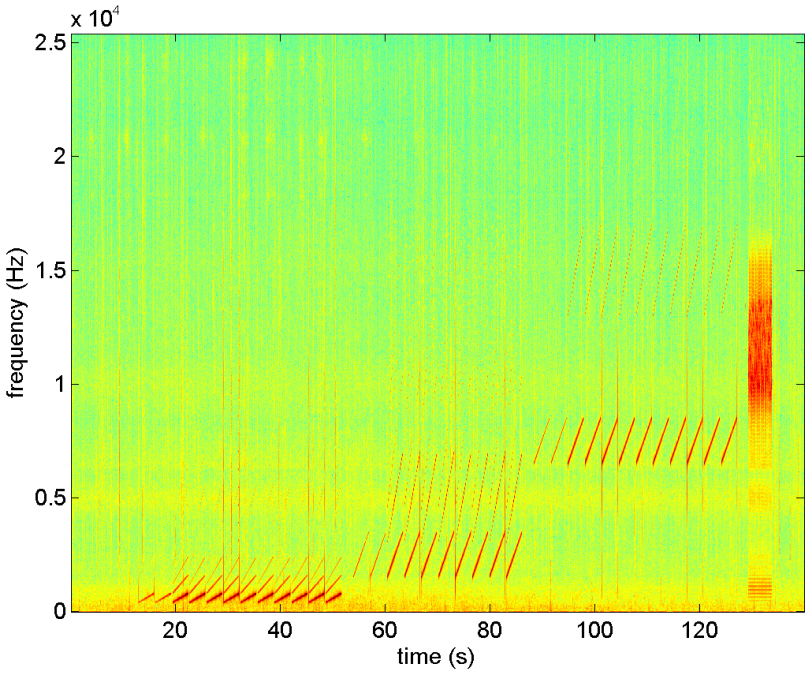

Figure 4.2: Probe signal sequence acquired by the monitoring hydrophone installed in the source mooring.

Fig 4.2 shows the spectrogram of the signal acquired by the monitoring hydrophone installed in the source mooring. One can observe that the emitting system generates several harmonics.

4.3 Received signals

The signal received at the 3 self-recording hydrophones were acquired at a sampling frequency of 50781 Hz and stored in "wav" file format. The acquired files were downloaded to individual directories for each run and hydrophone. The date of modification of each "wav" file is the system time (GMT) when the file was closed (end of the acquisition), except for the older self-recording hydrophone installed at the deepest position (Hyd #3), where that information appears in a separated text file (filelist.txt). There is no synchronization at sample level between hydrophones.

Figure 4.3 shows the received signal in hydrophone #2 (a) and the respective spectrogram (b). The multipath structure of the channel is presented in figure 4.4 where one can see the low-frequency (a) and medium frequency (b) pulse compressed received signal at hydrophone #2 and respective envelopes (c) and (d) of October 16, 11:30 GMT.

One can observe that the envelopes are relatively stable within the group, thus in further processing (see next chapter) they will be averaged. Due to the higher frequency band of the medium frequency signal the different arrivals are better resolved.

(a)

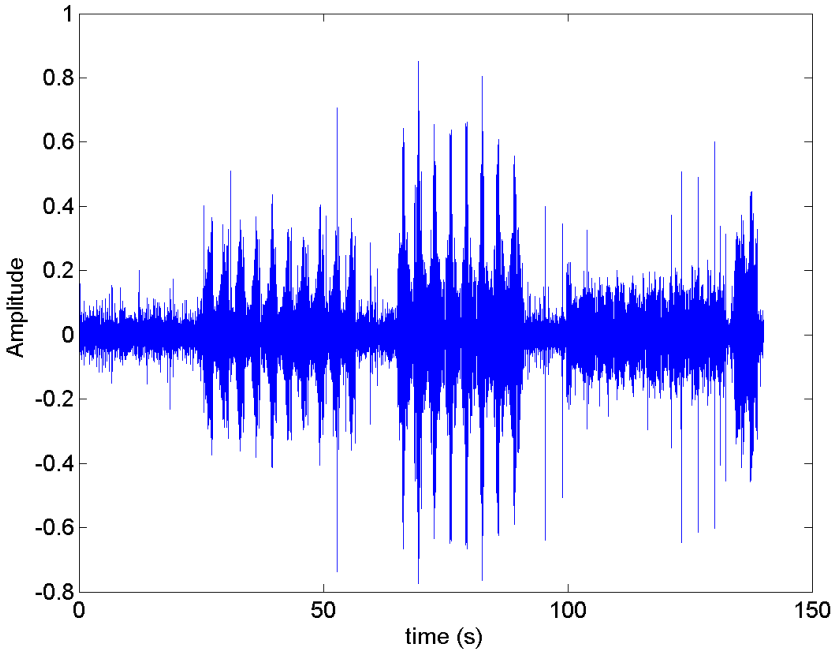

(b)

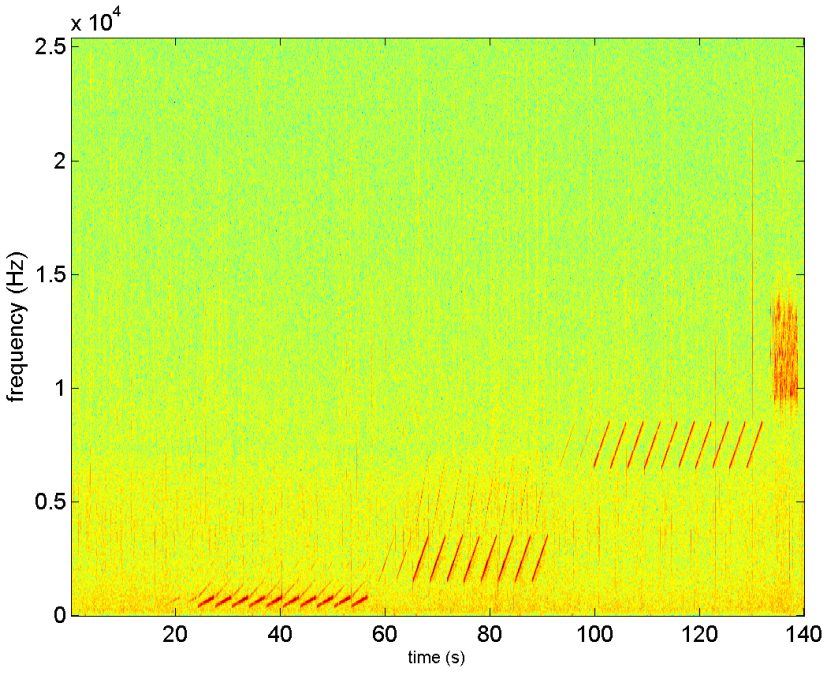

Figure 4.3: Sample of a signal sequence received at hydrophone #2 (a) and respective spectrogram (b)

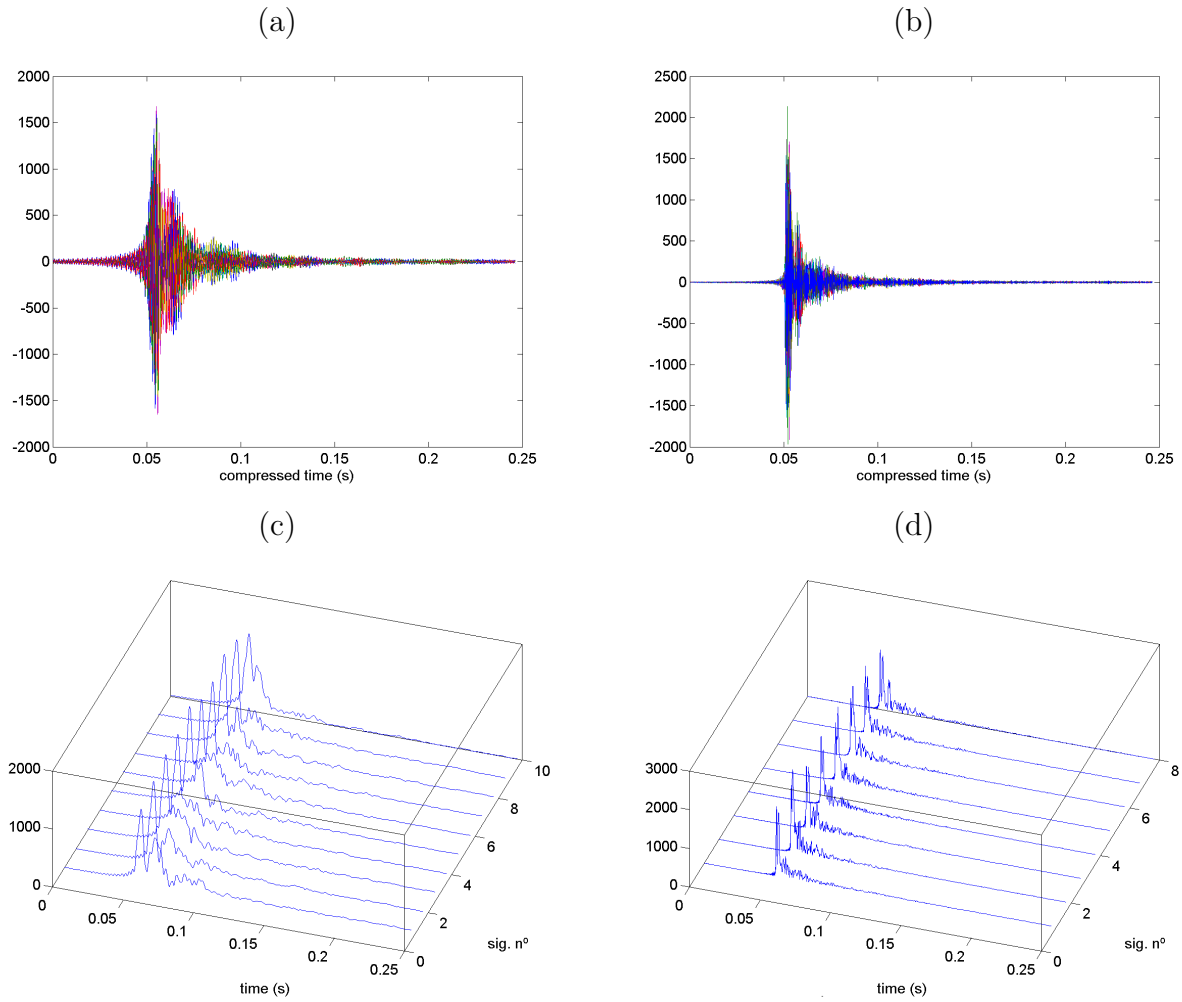

Figure 4.4: Pulse compressed low frequency (a) and medium frequency (b) chirps acquired October 16 at 11:10 (GMT) and respective envelopes (c) and (d)

Chapter 5

Preliminary channel characterization

5.1 Arrival patterns

The arrival patterns were computed by pulse compression, crosscorrelation between the received signal and the emitted signal, without considering the transfer function of the emitting system. The low and medium frequency signals were downsampled by a factor of 5 and the high frequency signals by a factor of 2, before pulse compression. The instantaneous envelopes of pulse compressed signals of a group were averaged after alignment by the maximum of crosscorrelation. The two low amplitude signals at the beginning of each block were discarded.

Figure 5.1 presents the arrival patterns computed from the signals acquired at hydrophone #2 covering about 2 period days from October 16 at 16:00 until October 18 at 14:30, with an interruption for hydrophones' battery exchange. The arrival patterns are presented in logarithmic scale to emphasize latter arrivals.

In low and medium frequency signals, figure 5.1 (a) and (b) respectively, one can see a remarkable difference between the time spread of the arrival patterns during the daylight (shorter) and night period (longer). The oxygen produced during the daylight period give rise to higher attenuation, thus latter arrivals, which suffer large number of bounces "can not be seen" in the arrival patterns. Also, arrival patterns show a higher variability during the daylight period than during the night, what can be explained by the fact that the oxygen production and the dissolution of oxygen in water varies along the day (mainly with irradiance) but it is not a linear and smooth process. At sunrise (daytime 17.2 and 18.2) there is an abrupt change in the arrival structure. At the sunset the change is smoother. When comparing the arrival patterns in the first day with those of the second day one observe (specially during night periods due to the stability of the arrivals) that in the second day latter arrivals have a greater strength, what can be explained by the lower wind speed during this day. Surface wind speed is a known cause of excess attenuation of latter arrivals. The influence of the wind speed on acoustic signal increases with frequency and it can be more relevant than the oxygen production, what explains that the acoustic signature of oxygen cannot be seen on high frequency signals (figure 5.1(c)).

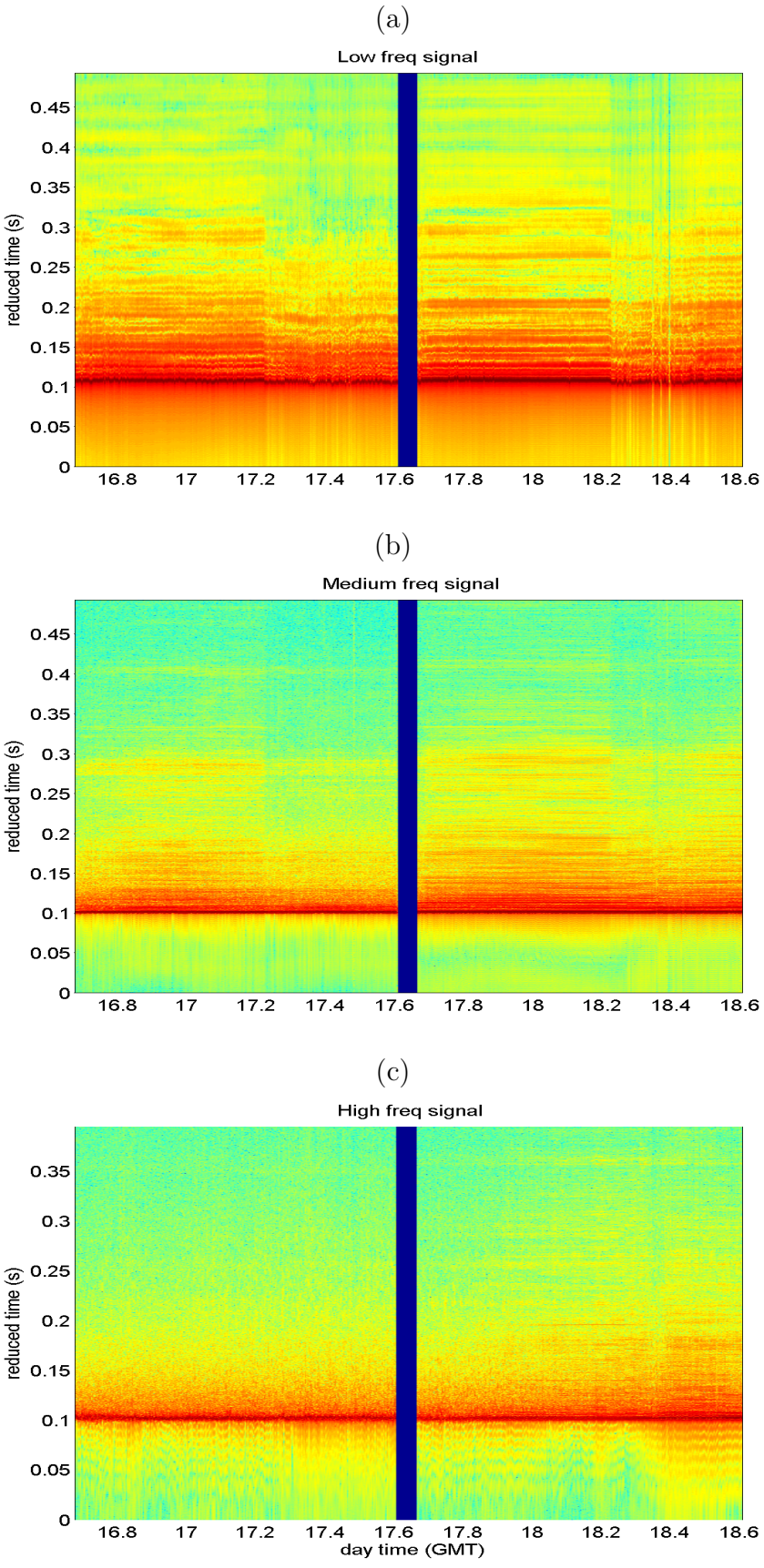

Figure 5.1: Arrival patterns of low frequency signals (a), medium frequency signals (b) and high frequency signals (c) acquired in hydrophone #2 from October 16 16:00 until October 18 14:30.

5.2 Analysis of arrival patterns

Figure 5.2 shows the ray paths predicted by cTRACEO propagation model [4] for hydrophone #2 (4 m above bottom) considering the experimental setup geometry in figure 2.2, an isovelocity sound speed profile (1546.5 m/s) and a sandy bottom (compressional bottom speed 1700 m/s, density 1.7 and compressional attenuation 0.7 dB/λ). One observes that ray #12 is a direct path, ray #11 has one bottom bounce, ray #13 has one surface bounce, rays #9,#10 and #11 have one bottom and one surface bounce (figure 5.3(a)). These arrivals correspond to earlier arrivals present in the measured arrival patterns. The second group of arrivals is a quadruplet (rays #15, #16, #8 and #7, figure 5.3(b)). The rays within this group have 2 surfaces bounces. The number of bottom bounces varies from 1 (ray #15) to 3 (ray#7).

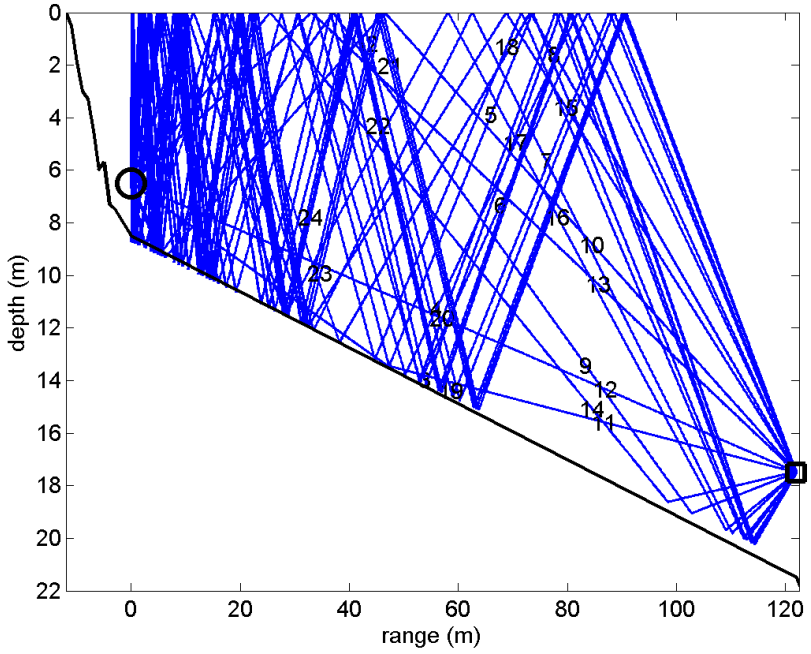

Figure 5.2: Eigenrays for hydrophone #2 modelled by cTRACEO. The label represents the eigenray number)

The latter groups of arrivals also have a quadruplet structure, being the number of bounces increased by one for each next quadruplet.

Figure 5.4 presents daylight (red line), night (black line) and daily (blue) averaged arrival patterns observed during last run of acoustic acquisition for the low frequency signal (a) and medium frequency signal (b), with superimposed amplitudes-delays predicted by the cTRACEO propagation model (green lines).

One can notice that the arrival patterns are very stable and their structure (number of arrivals and position) did'nt changed (visibly) with the time period considered. Moreover, there is a good agreement between the observed structure and the predicted one. The additional arrivals present in the arrival patterns, not accounted for by the propagation model, can by explained by rays reflected from the pier behind the source and other surrounding reflectors. Since, the medium frequency signal has a 2.5 times wider bandwidth than the low frequency signals the arrival patterns for the former present higher resolution than for the later. Also, the frequency response of the source in the medium frequency signal band is relatively flat, whereas for the low frequency signal is a slope with 20dB

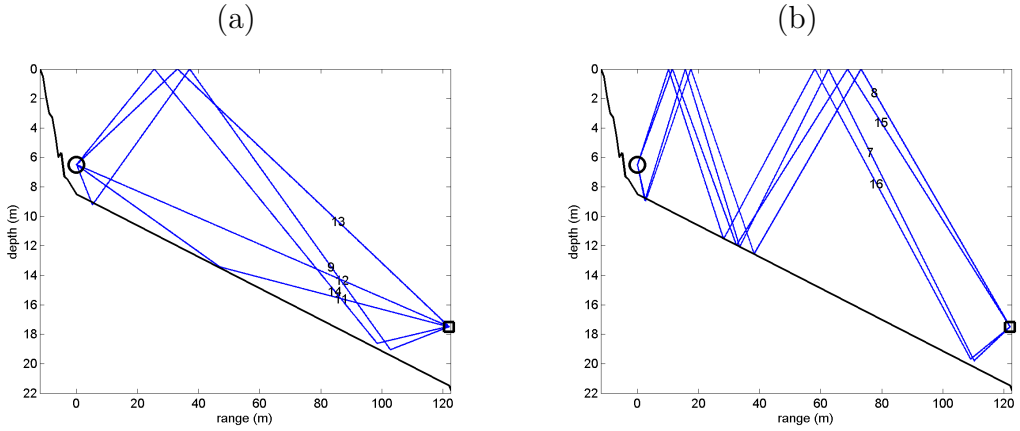

Figure 5.3: Engenray paths of early arrivals (a) and first quadruplet (b)

difference between the lowest and highest frequency, what reduces the effective bandwidth of the low frequency signal (see frequency response in Appendix A).

When comparing the time spread of the arrival patterns predicted by the model (about 50 ms) and that observed in figure 5.1 (more than 200 ms), one remarks that the latter is longer, what most likely is due to rays that are reflected in surrounding rocks (3D propagation effects).

However, maybe the most relevant feature observed for the purposes of oxygen estimation is that, in general, the amplitude of the daylight arrivals is smaller than the night arrivals, what seems to be highly correlated with the oxygen production. This can be observed also for latter arrivals (most of them not predicted by the propagation model) as can be seen in figure 5.5 for the medium frequency signals. Since latter arrivals have, in general, more interactions with the surfaces and longer propagation paths, the effect of the oxygen concentration should be more relevant in those rays (what is suggested in figure 5.1), however these rays are highly attenuated and are in the noise floor.

The behavior observed in the low and high frequency signals is not observed in the high frequency signals (figure 5.6), whereas the daylight arrivals presents higher amplitudes than night arrivals. One explanation could be that the wind speed is more relevant at those frequencies. However we should remark also that those arrival patterns are also stable during the considered periods.

The amplitude differences observed in the average arrival patterns for the different time periods in low and medium frequency signals suggest that it can be used to track the changes in oxygen on the water column and estimate the oxygen production. Next, figure 5.7 presents the low and medium frequency signals, the square of the amplitude of the arrival patterns integrated from 0.1 to 0.114 s, (received energy) for each group of transmissions during the whole second period of acquisition (16-18 October). The integration time corresponds to the two initial group of arrivals described previously. The dots represent a single value (corresponding to a group of transmissions), whereas the black lines represent the moving average of 6 single values (half-hour averaging time).

One can observe that during the night periods the energy received is higher than in the daylight periods. The variability of the received energy is higher during the daylight periods. Those features could be highly correlated with the photosynthesis and oxygen production and suggests that it can be used to evaluate the oxygen production of a seagrass meadow. One should remark that similar patterns were presented in fig. 4 of [5] for direct oxygen measurements using optodes during summer days in the same area. The general trend of increasing received energy during the period could be correlated with the decreasing wind speed.

(a)

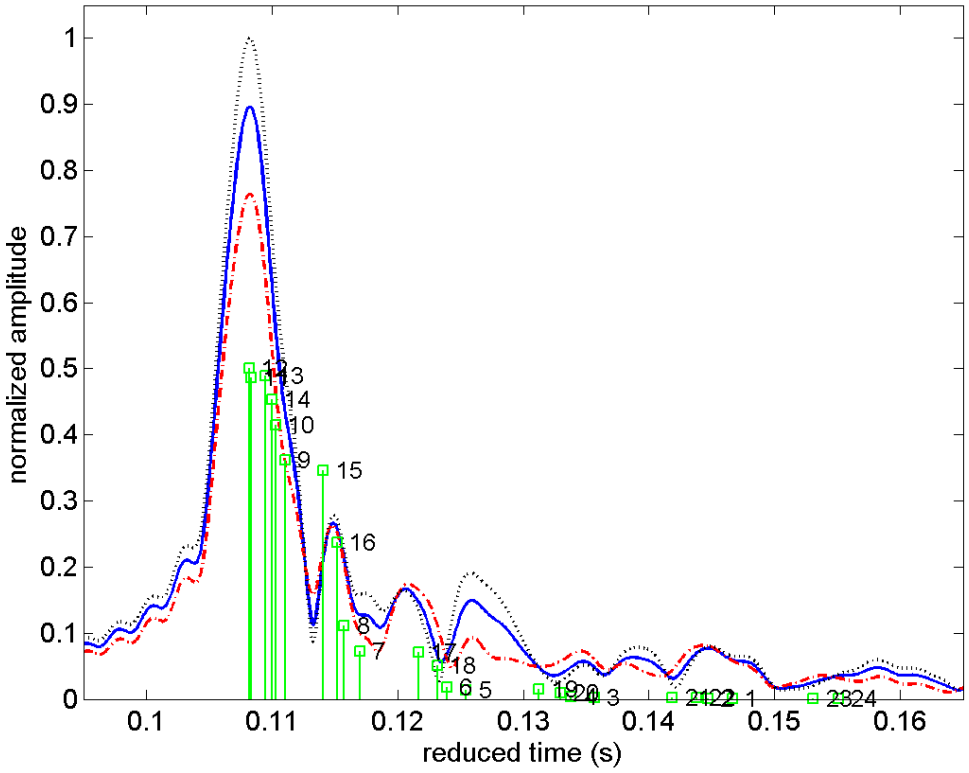

(b)

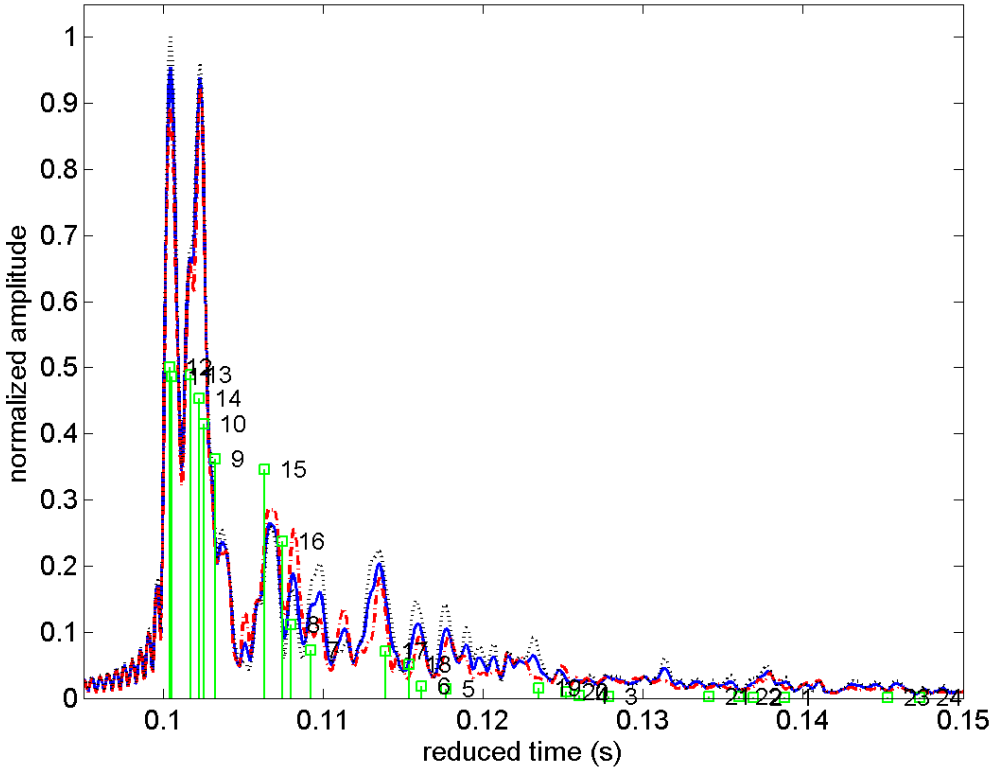

Figure 5.4: Average arrival patterns for run R17102011 (blue - all 4 arrivals, red - daylight arrivals, black - night arrivals) (a) low frequency signal (b) medium frequency signal with superimposed ray delays and amplitudes modeled by cTRACEO (green squares)

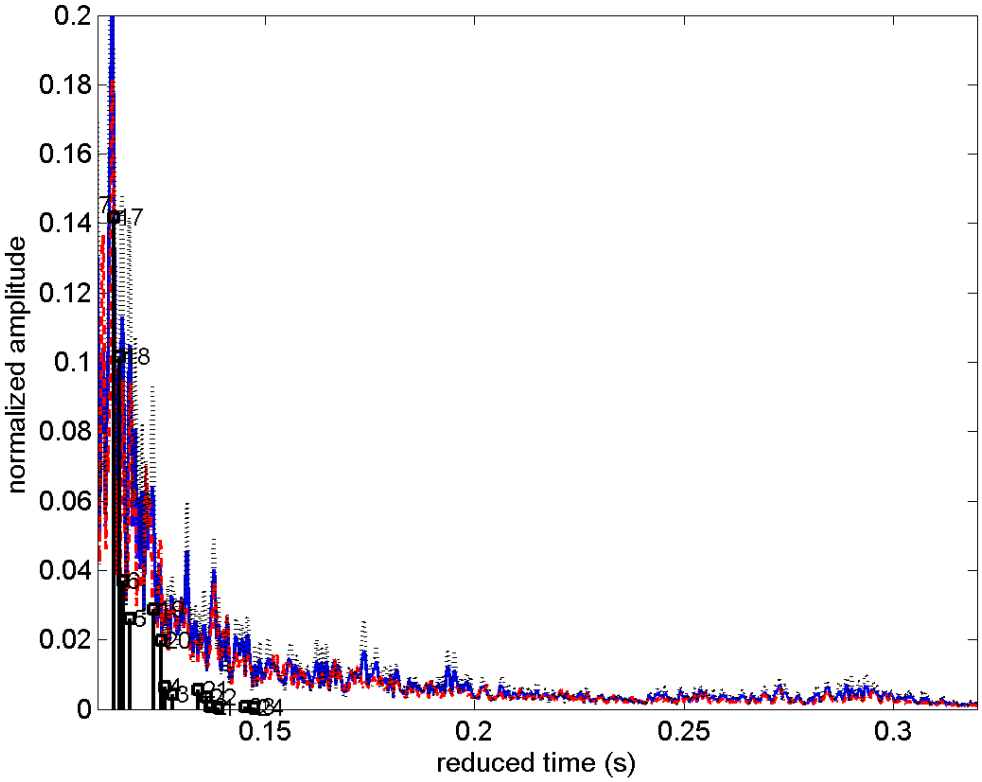

Figure 5.5: Zoom of the latter arrivals of figure 5.4(b)

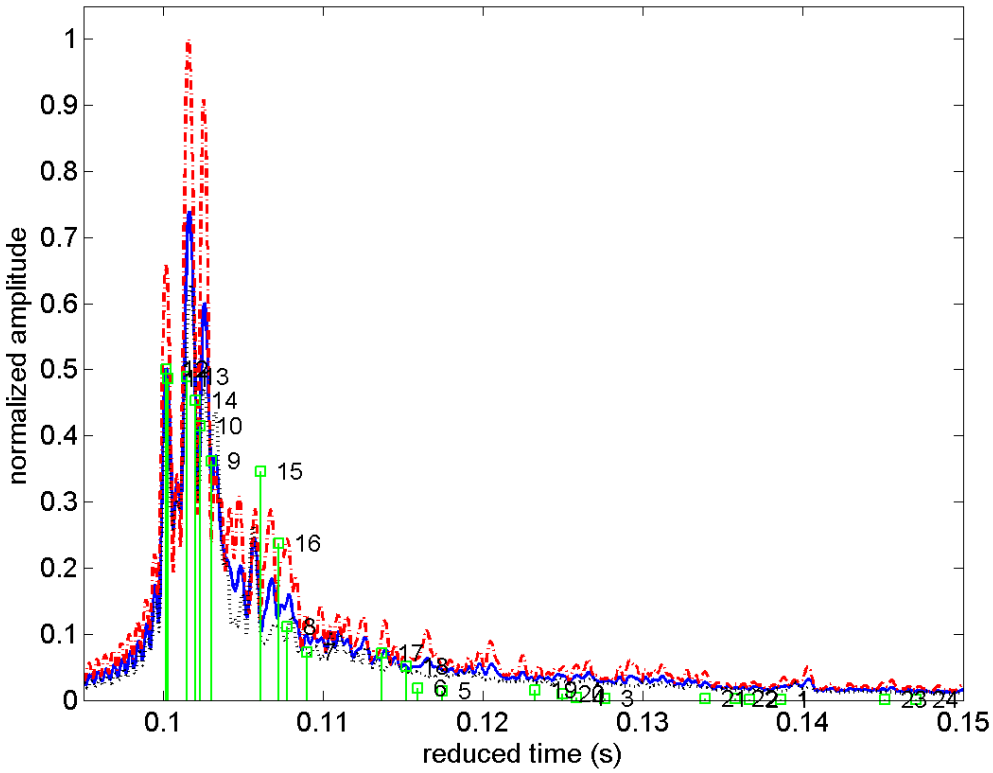

Figure 5.6: Average arrival patterns for run R17102011 (blue - all 4 arrivals, red - daylight arrivals, black - night arrivals) high frequency signal with superimposed ray delays and amplitudes modeled by cTRACEO (green squares)

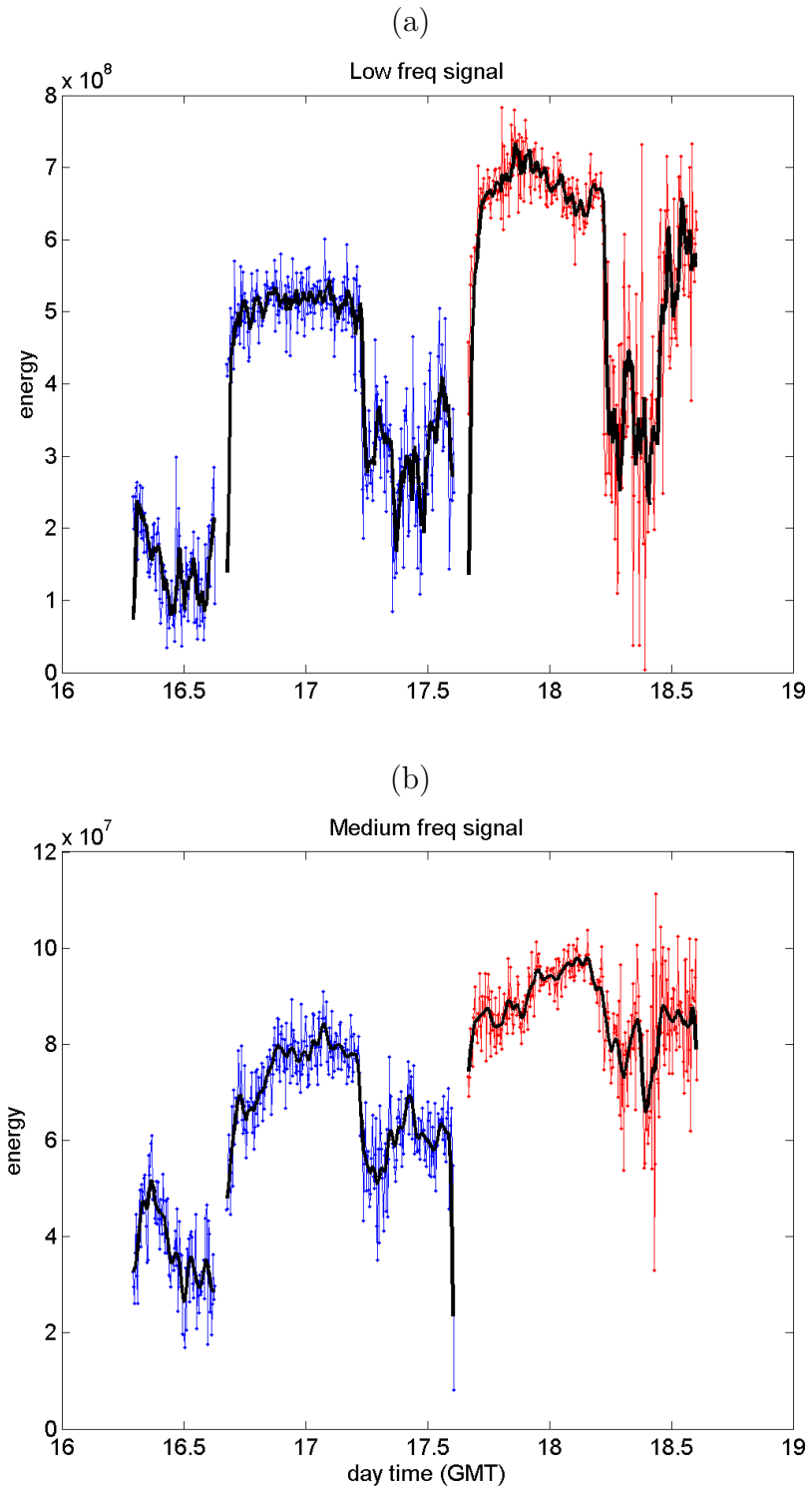

Figure 5.7: Time evolution of the energy received energy in hydrophone #2 for low frequency signals (a) and medium frequency signals (b). The dots represent the energy of a group of transmissions, whereas the black lines represent the a moving average of 6 groups of transmissions corresponding to half hour average

Chapter 6

Conclusions

This report presents the environmental and acoustic data acquired during the COST WS in STARESO for the purpose of developing an acoustic system for monitoring the oxygen production of a seagrass meadow. It was shown that the oxygen production in such a community gives rise to a visible acoustic signature that can be explored to evaluate and quantify the oxygen production. For signals in low frequency band (400-800 Hz) and medium frequency band (1.5-3.5 kHz) it was observed that during daylight periods the amplitude of the arrivals are smaller than those observed during night periods. This was not the case in high frequency signals (6.5-8.5 kHz), where the wind speed and surface waves can be more relevant for acoustic propagation than the variability of oxygen in the water.

Using a simple procedure to estimate the received power allowed to obtain figures of variability along time that seem to be highly correlated with oxygen production and show similar trend with oxygen measurements by optodes conducted in the same area [5].

Such oxygen measurements were also performed during the actual experiment, however those data will be available only after February 2012, when the optodes will be recovered. These data can be used to validate and calibrate the acoustic methods to estimate oxygen production.

Globally one can say that acoustic methods can potentially be used in a monitoring system to quantify the oxygen production of a seagrass meadow. Moreover, one can consider that such a system could simultaneously estimate the sound speed/temperature perturbations by acoustic means.

Appendix A

Sound source specifications

Lubell LL916C Underwater Speaker

The LL916 is an economical yet powerful piezoelectric underwater speaker developed, patented, and manufactured by Lubell Labs of Columbus Ohio. When used with optional PVi4B amplifier, the LL916 (and it's light-duty LL9816 counterpart) is capable of filling a 25 yard olympic pool with sound for lap swimming, a 50 meter Olympic pool for synchronized swimming, or a 500 meter distance in the open ocean for experiments. *No other brand compares!* The LL916 is provided with audio isolation transformer box with cord (see below), ready to connect to optional PVi 4B powered mixer & accessories.

- **Type:** Piezoelectric drive-piston tonpilz
- **Frequency Response:** 200Hz - 20kHz
- **Outlet Level:** 180dB/uPa/m @ 1kHz
- **Maximum Cable Voltage/Current:** 20 Vrms / 3A (100% duty cycle)
- **Operating Depth:** 6' recommended, 50' maximum
- **Finish:** Blue PVC
- **Cable:** 25' 18/3 PVC terminated with 3-pin Conxall 3182-3PG-524
- **Weight:** 15 lbs in air, 3 lbs in water
- **Size:** 9.0" diameter x 6.0" axial length (transducer); 10.750"x10.750"x7.750" (cage)
- **PDF Documents:** Data plot, general guide, printable brochure
- **Limited Warranty:** 5 years
- **Retail Price: $1512** (Includes AC205C inline transformer box); **$1588** (Includes AC203E transformer box with air speaker jack & control)
- **Accessories:** PVi4B 80W powered mixer ($179); SX80BE 8" PA speaker ($229) or Quadra10 10" PA speaker ($269); H14-25' air speaker cord ($33) or H14-50' air speaker cord ($43); SS7761B tripod stand for Quadra10 ($69); ST95MKII hand mic with 20' cord ($49); ATW-701/H wireless headset mic ($299); ATW-702 wireless hand mic ($269); CD-A550 CD/tape deck ($389).
- ***School, dealer, quantity, and cash discounts available***

Lubell Labs Inc.
21 N. Stanwood Rd.
Columbus, Ohio 43209 USA
(614) 235-6740 tel
lubell_labs@wowway.com

Lubell Labs LL916 TVR & Z Plots

Notes: LL916 Transmit Voltage Response (dB/uPa/m @ 1 volt) -- add ~26dB to obtain SPL @ 20 Vrms drive. Unit tested at 28' depth at NUWC Dodge Pond.

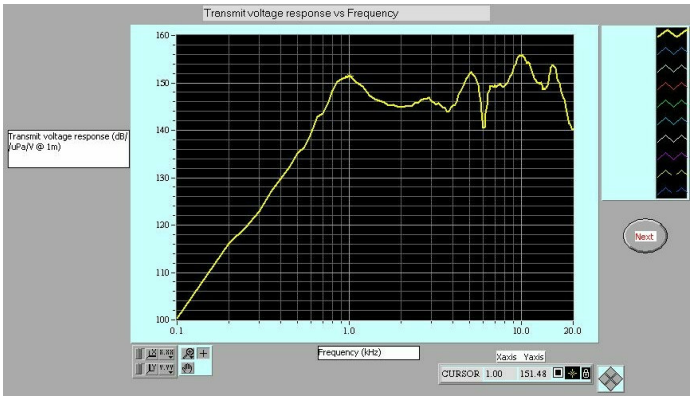

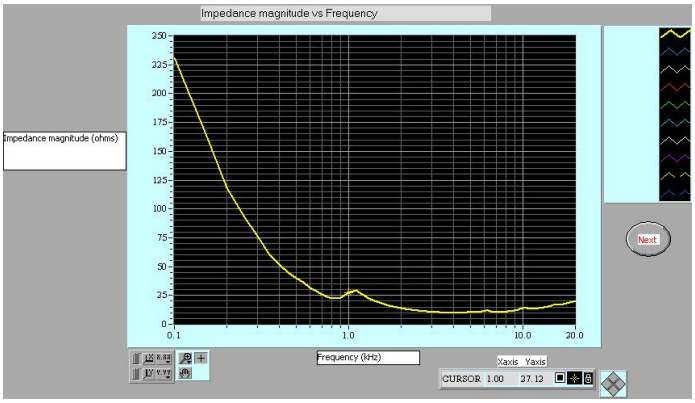

Appendix B

Self-recording digital hydrophone digitalHyd SR-1 specifications

digitalHyd SR-1

Self-Recording Digital Hydrophone

Specifications

- Transducer Voltage Sensitivity:
  -194 dBV re 1 µPa
- Voltage Gains (Programmable Gain Amplifier):
  0 dB, 6 dB, 12 dB, 18 dB, 24 dB, 30 dB, 36 dB
- Input Sound Pressure Level Range:
  46.3 dB re 1 µPa to 172.5 dB re 1 µPa
- Sample Frequency:
  50.781 kHz / 101.562 kHz (selectable)
- Usable Acoustic Band:
  1 Hz to 24.9 kHz / 1 Hz to 49.8 kHz
- Sample Resolution:
  24 bits acquisition, 16 bits storage
- Memory Card Capacity:
  up to 8GB (field replaceable)
- Real Time Clock:
  ± 64 seconds per year
- Battery:
  3.7V_{DC}, 2400mAh, Lithium-Ion 18650
- Battery Life:
  up to 10h in continuous acquisition
  up to 500h in stand-by (using timetable acquisition)
  expandable with larger battery packs
- Maximum Depth:
  designed to 100m
- Operation Temperature Range:
  0 °C to 40 °C
- Case Material:
  Delrin
- Case dimension:
  50 x 323 mm (diameter x length)
- Weight:
  0.18 kg (in water), 0.77 kg (in air)

Description

The digitalHyd SR-1 is an autonomous recording device designed for user-friendly operation in underwater acoustic signal acquisition activities. Its compact construction and functionalities allows for the implementation of efficient measurement strategies, thus, avoiding the requirement of large operational human and material resources for deployment and recovery.

The digitalHyd SR-1 records signals in the frequency band from 1Hz to 24.9kHz or 1Hz to 49.8kHz, depending on selected sampling frequency. These signals are stored on a removable memory card, using 16-bit resolution, and can be opened by conventional media players and signal processing applications. All acquisition information including date, time and gain are available in the header of the files for later analysis. The acquisition can start as soon as the device is powered up or at predefined scheduled dates and times. Programmable parameters include file duration, PGA gain and start-up times, among others. The configuration of all parameters is performed through a USB interface with access compatibility from various types of operating systems.

The digitalHyd SR-1 is powered by a rechargeable lithium-ion battery and is able to remain on for up to 10 hours of continous acquisition, or various days in stand-by. Battery and memory card are field replaceable, to allow for quick redeployments of the Hydrophone. Optional battery extension packs are available on demand, expanding the SR-1 to the user required autonomy.

Applications

- Underwater Noise Monitoring
- Bioacoustics
- Underwater Acoustics Research
- Acoustic Field Calibration

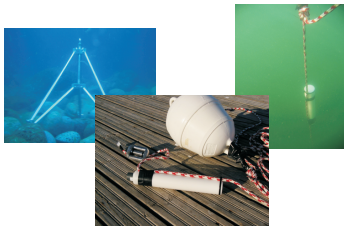

address: **Marsensing Lda**, Centro Empresarial - Pav. A5, Campus de Gambelas, 8005-139 Faro, Portugal
tel: +351 913 729 660
url: www.marsensing.com
e-mail: contact@marsensing.com

Bibliography

[1] J. P. Hermand, P. Nascetti, and F. Cinelli, "Inverse acoustical determination of photosynthetic oxygen productivity of posidonia seagrass," *Experimental Acoustic Inversion Methods for Exploration of the Shallow Water Environment*, 2000.

[2] J.-P. Hermand, "Photosynthesis of seagrasses observed in situ from acoustic measurements," in *Proc. Int. Conf. IEEE/EOS Oceans'04*, 2004.

[3] M. Saleiro, "Portable acoustic source unit (pasu)," SiPLAB/University of Algarve, Tech. Rep. 05/09, March 2009.

[4] O. Rodríguez. (2011) Trace model. [Online]. Available: http://www.siplab.fct.ualg.pt/models.shtml

[5] W. Champenois and A. Borges, "Seasonal and inter-annual variations of community metabolism rates of a posidonia oceanica seagrass meadow," *Limnology and Oceanography Bulletin accepted*.